Analytical Methods

Accepted Manuscript

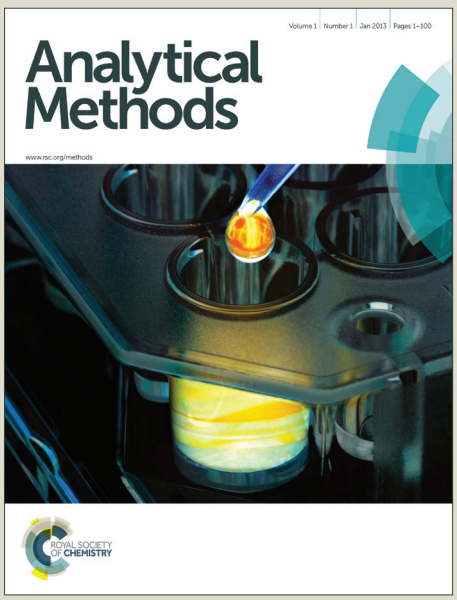

ROYAL SOCIETY OF CHEMISTRY

www.rsc.org/methods

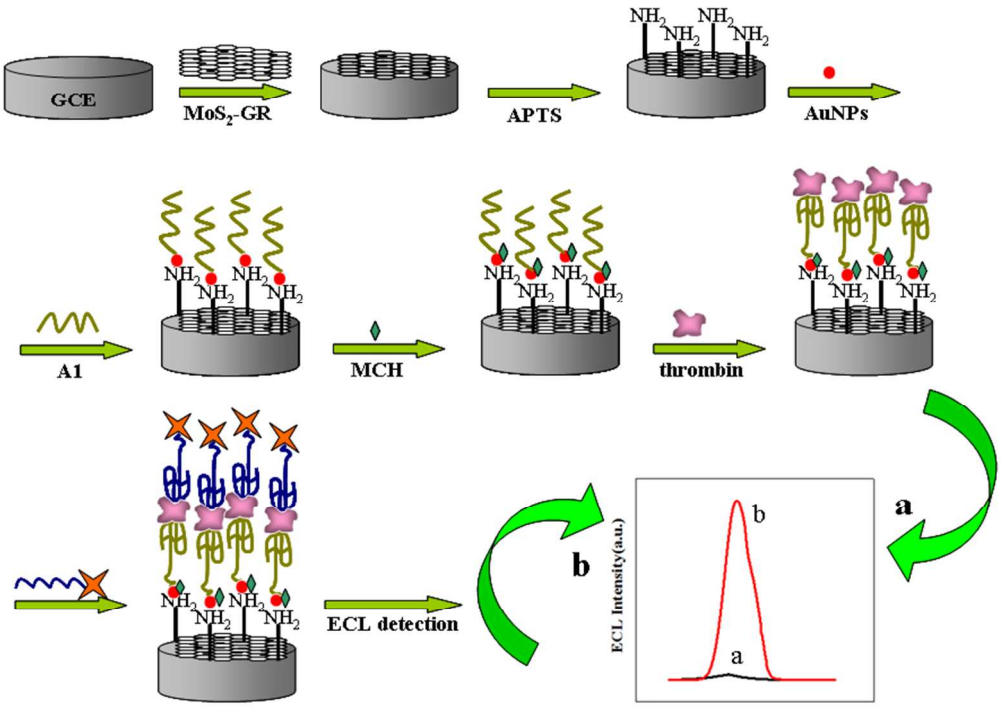

graphical abstract
75x53mm (300 x 300 DPI)

Cite this: DOI: 10.1039/c0xx00000x

www.rsc.org/xxxxxx

ARTICLE TYPE

Novel sandwich electrochemiluminescence aptasensor based on molybdenum disulfide nanosheets–graphene composites and Au nanoparticles for signal amplification

Yan–Ming Liu[*a], Min Zhou[a], Ying–Ying Liu[a], Ke–Jing Huang[a], Jun–Tao Cao[a], Jing–Jing Zhang[a], Gui–Fang Shi[a], Yong–Hong Chen[b]

Received (in XXX, XXX) Xth XXXXXXXXX 20XX, Accepted Xth XXXXXXXXX 20XX
DOI: 10.1039/b000000x

In this work, we constructed a novel sandwich electrochemiluminescence (ECL) aptasensor for sensitive detection of thrombin based on molybdenum disulfide nanosheets–graphene (MoS_2–GR) composites and Au nanoparticles. In the protocol, MoS_2–GR composites were firstly synthesized and assembled on the glassy carbon electrode (GCE) to promote the electron transfer. Subsequently, gold nanoparticles (AuNPs) were covered on the electrode to improve the immobilized amount of aptamer1 (Apt1) and could further amplify the ECL signal as well. Afterwards, Apt1 was conjugated to the electrode via Au–S bond. Finally, the target thrombin and the quantum dots labeled aptamer2 (QDs–Apt2) as signal probe were successively attached to the GCE to fabricate a sandwich ECL aptasensor. With the excellent features of the MoS_2–GR composites, AuNPs, and sandwich structure, multiple signal amplification for the ECL aptasensor has been achieved. The ECL intensity depended linearly on the logarithm of the thrombin concentration in the range from 0.02 to 5.0 pM and a detection limit of 1.3 fM (S/N = 3). Furthermore, the aptasensor was successfully applied to the determination of thrombin in human plasma with the recoveries of 90.0–102.4% and the RSDs of 2.1–3.7%. The protocol could serve as a new tool for protein detection in biochemical analysis.

Introduction

Aptamers are single–stranded oligonucleotides that are being used in various novel scientific fields as recognition probes, such as protein analysis, disease diagnosis and development of biosensor.[1, 2] Aptamers have many advantages over traditional recognition molecules, for example simpler synthesis, easier storage, better reproducibility, lower cost, higher specificity, and wider applicability.[3, 4] Aptamers can be also easily chemically modified with signal moieties and further enhance their biochemical stability. Numerous aptamer–based biosensors (aptasensors) have been documented for detection of small molecules,[5] metal ions,[6] and proteins.[7] The different detection techniques for aptasensors were utilized including fluorescence,[8] colorimety,[9] chemiluminescence,[10] and electrochemiluminescence (ECL).[11] Among them, ECL aptasensor has attracted much attention because of its better sensitivity, selectivity, and wider linear range.[12, 13] Wang et al. developed a label–free bifunctional ECL aptasensor for detection of adenosine and lysozyme.[14] Yu et al. reported an ECL aptasensor for tumor cells assay with a detection limit of 78 cells mL^{-1}.[15]

ECL is a powerful detection technique due to its remarkable features, for example high sensitivity, low background, simple instrumentation and rapidity. The ECL has been applied in the analysis of macrolide antibiotics,[16] anesthetics[17] and hemoglobin.[18] ECL sensors based on quantum dots (QDs)[19, 20] have been developed for the detection of metal ions,[21] DNA molecular,[22, 23] amino acid,[24] and protein.[25] CdSe–ZnS core–shell QDs, one kind of biocompatible semiconductor nanoparticles, has been used in the detection of protein[26] and cancer cells.[27]

Most recently, the 2D nanomaterials, especially layered transition–metal dichalcogenides, have attracted great interests in the fields of electrochemistry because of their excellent electrochemical performance, especially in the fields of catalysts, sensors, electrode materials for capacitors, and lithium–ion batteries. MoS_2, a typical family member of transition–metal dichalcogenides, has a sandwich structure similar to GR, which consists of three stacked atom layers (S–Mo–S) held together by Van der Waals force.[28] Due to the distinctive layer structure and electronic properties, MoS_2 has been used in many fields, including electrode materials for lithium battery[29] and capacitor[30] and potential hydrogen storage media.[31] However, few attentions have been put into its application as an electrode material for sensors because the electronic conductivity of MoS_2 is still lower compared to graphite/graphene. The combination of MoS_2 and other conducting materials may overcome this deficiency, such as graphene (GR).

GR, a flat monolayer of carbon atoms bonded through sp^2 hybridization, has many outstanding properties comprising good

electronic transport properties, high conductivity, large surface area and strong mechanical properties.[32] However, the surface of GR needs functionalization or chemical modification to improve its dispersible in aqueous solution. From this viewpoint, the composite functional nanomaterials by combination of MoS_2 and GR might bring unexpected novel properties.[33] Thus, the layered MoS_2–GR composites have been synthesized and used to detect small molecule (acetaminophen) with a detection limit of 2.0×10^{-8} M by our group.[34]

Thrombin is a kind of important enzyme in blood responsible for coagulation and related to many physiological processes. It plays a major role in a number of cardio–vascular diseases, and it is thought to regulate many processes in inflammation and tissue repair at the vessel wall.[35] Many methods for thrombin detection have been developed. Sun et al. fabricated an electrochemical aptasensor for thrombin detection with the detection limit of 1.56×10^{-14} M.[36] Wang et al. described a $Ru(phen)_3^{2+}$–based ECL aptasensor for thrombin detection with a detection limit of 4.0×10^{-13} M.[37]

In this work, a novel, facile and ultrasensitive ECL aptasensor was constructed based on MoS_2–GR composites for thrombin detection. The aptasensor with sandwich structure was designed by self–assembling method via thrombin–aptamer recognition reaction. With the excellent features of the MoS_2–GR composites, AuNPs, and sandwich structure, the as–prepared ECL aptasensor exhibits highly ECL response and good stability. The results obtained indicate that the constructed aptasensor could be used for the sensitive and selective detection of thrombin.

Experimental

Reagents and materials.

Human thrombin was purchased from Sigma–Aldrich (St. Louis, MO, USA). Two DNA sequences (Apt1, 5′–SH–$(CH_2)_6$–TTT TTT TTT TTT TTT GGT TGG TGT GGT TGG–3′; Apt2, 5′–NH2–$(CH_2)_6$–TTT TTA GTC CGT GGT AGG GCA GGT TGG GGT GAC T–3′) were obtained from Sangon Biotechnology Co., Ltd. (Shanghai, China). Hydrogen tetra chloroaurate (III) trihydrate ($HAuCl_4$•$3H_2O$) was from Alfa Aesar. 6–Mercapto–1–hexanol (MCH) was from Tianjin Heowns Biochem LLC (Tianjin, China). Graphite powder, Na_2MoO_4•$2H_2O$, and L–cysteine were from Shanghai Chemical Reagent Corporation (Shanghai, China). The carboxyl–modified core–shell CdSe–ZnS QDs were from Wuhan Jiayuan Quantum Dots Co., Ltd. (Wuhan, China). All reagents were of analytical–reagent grade. The water (18.2 MΩ•cm) used was processed with an ultrapure water system (Kangning Water Treatment Solution Provider, China).

Apparatus.

Cyclic voltammetry (CV) and electrochemical impedance spectroscopy (EIS) measurements were carried out with a RST5200 electrochemical workstation (Zhengzhou Shiruisi Technology Co., Ltd., China). The ECL signal was collected with the photomultiplier tube (PMT, CR 120, Binsong Photonics, China) and BPCL ultra weak luminescence analyzer (Institute of Biophysics, Chinese Academy of Science, Beijing, China) and then recorded and processed with a computer using BPCL software. All electrochemical experiments were performed with a conventional three–electrode system. The morphologies of the composites were recorded on a JEM–2100 transmission electron microscope (TEM) and a Hitachi S–4800 scanning electron microscope (SEM). X–ray powder diffraction (XRD) pattern was operated on a Japan RigakuD/Maxr–A X–ray diffractometer equipped with graphite monochromatized high–intensity Cu Kα radiation (λ = 1.54178 Å). Raman spectrum was executed on an England RENISHAW–INVIA Raman spectrometer with 514.5 nm laser and spectra range 80–9400 cm^{-1}.

Preparation of graphene oxide (GO), MoS_2–GR composites and MoS_2.

In a typical experiment, GO was prepared by the modified Hummer's method.[38] MoS_2–GR composites were prepared by L–cysteine–assisted solution–phase method according to our previous work.[34] 60 mg GO was dissolved in 50 mL water and then 0.3 g Na_2MoO_4•$2H_2O$ was added. After ultrasonication for 20 min, the pH of the solution was adjusted to 6.5 with 0.1 mol•L^{-1} NaOH and then addition of 0.8 g of L–cysteine and 30 mL water. The above mixture was transferred into a 100 mL Teflon–lined stainless steel autoclave and heated at 180 ºC for 48 h. After cooling naturally, the black precipitates were collected by centrifugation, washed with water and ethanol, and dried in a vacuum oven at 80 ºC for 24 h. Besides, the preparation of MoS_2 was similar with MoS_2–GR without addition of GO.

Preparation of QDs–aptamer conjugates.

CdSe–ZnS QDs were conjugated to Apt2 using the N–(3–dimethylaminopropyl)–N'–ethylcarbodiimide hydrochloride (EDC) and N–hydroxy–succinimide (NHS) as coupling agent.[39] First, 5 μL 8 μM QDs was mixed with 80 μL 10 mM pH 7.4 PBS containing 1 mM EDC and 5 mM NHS, and reacted for 0.5 h at room temperature to activate the carboxyl–terminated surface of the CdSe–ZnS QDs. Then, 5 μL 10 μM Apt2 was added to the above mixture and reacted for 2 h at room temperature. The products were purified by dialyzing against water with a cellulose ester membrane bag. Then QDs–Apt2 was obtained and stored at 4 ºC before use.

Fabrication of the ECL aptasensor.

The ECL aptasensor was fabricated based on MoS_2–GR composites by layer–by–layer self–assembly method. The MoS_2–GR composites could significantly improve the loading capacity and conductivity of the GCE. AuNPs was prepared according to our previous work.[40] The GCE (3–mm–diameter) was polished with 1, 0.3, and 0.05 μm alumina slurry sequentially. After sonicating in ethanol and water in turn, the GCE was allowed to dry at room temperature. Then, 10 μL MoS_2–GR composites was trickled onto the GCE, then dried and soaked in 3–aminopropyltriethoxysilane (APTS) solution (2%, v/v) for 0.5 h to introduce the amine functional groups. Prepared in this way, the substrate surface was covered with positively charged APTS that readily adsorbed AuNPs with negative charge. After immersed into the AuNPs solution for 2 h, 5 μL Apt1 was dropped on the modified GCE to form Au–S bond. Subsequently, the electrode was rinsed with 10 mM pH 7.4 PBS and treated with 1 mM pH 7.4 MCH solution containing 10 mM PBS and 1 M NaCl to block up the nonspecifically bound oligonucleotides. Later, 10 μL thrombin was dropped onto the surface of the modified GCE and incubation at 37 ºC for 1 h. After washed with

Tris–HCl and dried, the GCE was immediately covered with 5 μL QDs–Apt2 solution at room temperature for 2 h. The above process is described in Scheme 1.

Results and discussion

Characterization of MoS_2–GR.

The MoS_2–GR composites were well characterized by SEM, TEM, XRD and Raman. SEM image of GR sheets (Fig. 1A) reveals that the sheets are thin and smooth. It also can be seen that the single layered GR displays transparent two–dimensional sheets structure look like thin silk veil waves from the TEM image of GR in Fig. 1B. The SEM image of the MoS_2–GR composites shown in Fig. 1C reveals that the composites aggregate into particles with a few hundred nanometer in size with a 3D architecture. This 3D structure increases both the loading capacity for guest molecules and the stability of composites due to superstrength of GR. From the TEM image of MoS_2–GR composites (Fig. 1D), it can be observed that the layered MoS_2 is supported on the single layered GR surface and no apparent aggregation of the layered MoS_2. The HRTEM image of MoS_2–GR inset in Fig. 1D shows that a series of parallel lines embedded in the surface, indicating that the layer structure of the products is overlapped each other. The numbers of layer are between 3 and 17.

The XRD patterns of layered MoS_2–GR composites (curve a) and MoS_2 (curve b) were illustrated in Fig. 2A. For MoS_2–GR composites, the peak at 24.1° is corresponding to the (002) crystal plane of GR, and the peak at 14.4°, 38.7° and 60.9° could be well–assigned to the (002), (100) and (110) planes of MoS_2, respectively. When 2θ = 14.4°, the interlayer distance is estimated to be 0.62 nm (2dsinθ = nλ). The characteristic peaks of MoS_2–GR composites also appear in Raman spectra. As shown in Fig. 2B, the peaks at 379 cm^{-1} and 404 cm^{-1} for MoS_2–GR in curve a are attributed to the MoS_2 (curve b) and peaks at 1327 cm^{-1} and 1598 cm^{-1} are assigned to the D and G peaks of GR (curve c), respectively.[28, 41] These results indicate that the MoS_2–GR composites have been synthesized successfully.

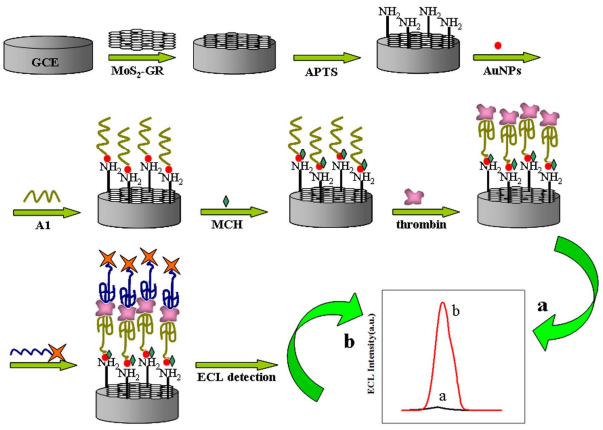

Scheme 1 Schematic diagram of the fabrication process of the ECL aptasensor.

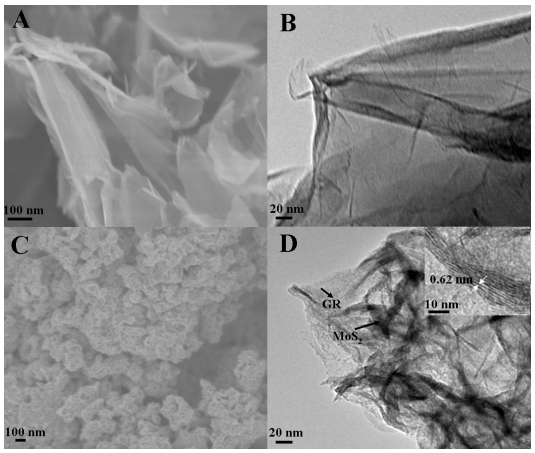

Fig. 1 SEM images of GR (A) and MoS_2–GR (C); TEM images of GR (B) and MoS_2–GR (D). Inset in (D): HRTEM of MoS_2–GR.

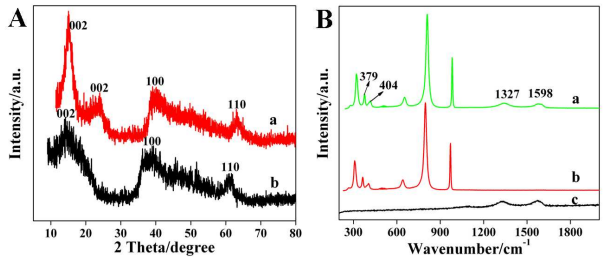

Fig. 2 (A) XRD patterns of MoS_2–GR (a) and MoS_2 (b); (B) Raman spectra of MoS_2–GR (a), MoS_2 (b) and GR (c).

The electrochemical and ECL behavior.

CV is an effective and convenient tool to investigate the changes of the electrode behavior after modified different materials. The CV curves of stepwise modified electrodes were shown in Fig. 3A. When the bare GCE (curve a) was firstly treated with MoS_2–GR, the peak current obviously increased due to the good conductivity of MoS_2–GR (curve b). The peak current further increased with AuNPs modification (curve c). When Apt1 was immobilized on the as–prepared GCE surface, the peak current decreased (curve d) because the aptamer can hinder the electron transfer. And the peak currents of both thrombin/Apt1/AuNPs/MoS_2–GR/GCE (curve e) and QDs–Apt2/thrombin/Apt1/AuNPs/MoS_2–GR/GCE (curve f) were further decreased. The decrease is ascribed to the addition of thrombin and Apt2 with nonconductive properties. The results indicate that the aptasensor is well fabricated.

EIS experiments were carried out to give further information on the impedance changes of the electrode surface in the modification process. The electrode impedance can be calculated on the basis of the Randles equivalent circuit shown in Figure 3B (inset). In the terms of EIS, $Fe(CN)_6^{3-/4-}$ was utilized as the redox probe and the semicircle diameter in the impedance spectrum equals the electron–transfer resistance, R_{et}. It is observed that the electron transfer resistance of the bare GCE was about 50 Ω (curve a). When the bare GCE was modified with MoS_2–GR and AuNPs sequentially, the resistance values decreased to 35 Ω (curve b), and 30 Ω (curve c), respectively, implying that the MoS_2–GR and AuNPs were excellent electric conducting materials and accelerated the electron transfer. After the

immobilization of Apt1, thrombin and QDs–Apt2 successively, the resistance values increased to 110 Ω (curve d), 200 Ω (curve e) and 320 Ω (curve f), respectively, this was because the introduction of Apt1, thrombin and QDs–Apt2 greatly inhibits the electron transfer of the redox probe on the electrode surface. The results obtained by EIS method are consistent with those from CV measurement, confirming the successful fabrication of the electrode device.

In this work, we constructed a sandwich–type ECL aptasensor based on CdSe–ZnS QDs to detect thrombin. ECL signal at each immobilization step was also recorded and illustrated in Fig. 3C. QDs used in this work are a good ECL emission reagent. Thrombin has two binding sites and it could be able to link two aptamers. The carboxyl–modified QDs could be conjugated with amino–group–modified Apt2 by coupling agent to form QDs–Apt2. In the absence of QDs–Apt2, thrombin bound to the Apt1 produces a weak ECL signal (Fig. 3C(a–e)). However, in the presence of QDs–Apt2, QDs–Apt2 used as ECL signal reporter could bind to thrombin and produce an obviously increased ECL signal (Fig. 3C(f)). In addition, the increase of ECL signal depends on the amount of QDs–Apt2, which is proportional to the amount of thrombin. So ECL of QDs in this work could be used in the quantitative analysis of thrombin (as probe). $K_2S_2O_8$ was chosen as coreactant in our work. The possible ECL mechanism[42] could be described as follows:

$$QDs + e^- \rightarrow QDs^-\bullet \quad (1)$$

$$S_2O_8^{2-} + e^- \rightarrow SO_4^{2-} + SO_4^-\bullet \quad (2)$$

$$QDs^-\bullet + SO_4^-\bullet \rightarrow QDs^* + SO_4^{2-} \quad (3)$$

$$QDs^* \rightarrow QDs + h\nu \quad (4)$$

The GR based aptasensor was also fabricated with the same procedure and used to detect the thrombin with the same analytical process. In comparison with GR based aptasensor, the ECL intensity of MoS_2–GR based aptasensor was greatly enhanced. The result indicates that MoS_2–GR composites were more powerful for the ECL biosensing, due to its large loading capacity and excellent conductivity.

The ultrasensitive detection of thrombin.

The fabricated ECL aptasensor was used to detect different concentration of thrombin (see Fig. 3D). In quantitative analysis, the linear range could be determined by the relation between signal intensity and concentration of analytes[14,40] or the relation between signal intensity and logarithm of concentration of analytes[26,44]. In this work, we found that the ECL intensity is proportional to the logarithm of thrombin concentration from 0.02 to 5.0 pM with a lower detection limit of 1.3 fM (S/N = 3). The linear equation was I = 33925.33 + 2364.12 log$C$, and the correlation coefficient is 0.993. Compared with other sensors reported previously (Table 1), the layered MoS_2–GR composites is firstly used to construct the ECL aptasensor and the proposed ECL aptasensor exhibits a lower detection limit and wider linear range.

The stability of the aptasensor was tested. Fig. 4A exhibits the ECL intensities of the aptasensor under consecutive potential scans from 0 to –1.7 V for 12 circles. The ECL signals are very high and stable (RSD, 1.1%), suggesting that this aptasensor is very suitable for ECL detection. To investigate the selectivity of the aptasensor, control experiments were performed using three similar proteins: 2.0×10^{-3} M HSA (column a), 1.0×10^{-6} M

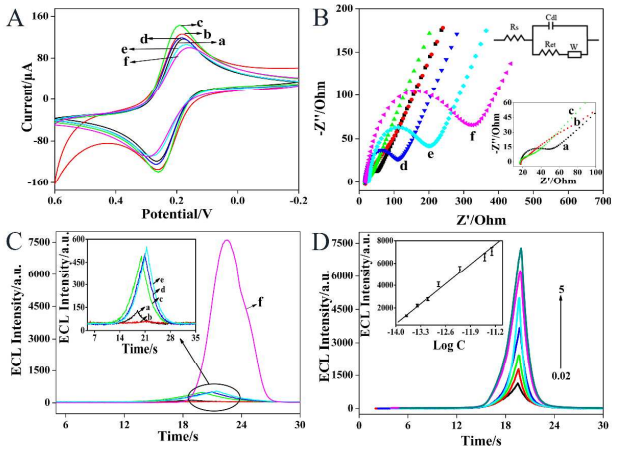

Fig. 3 (A) CV, (B) EIS, and (C) ECL intensity of stepwise modification at (a) bare GCE, (b) MoS_2–GR/GCE, (c) AuNPs/MoS_2–GR/GCE, (d) Apt1/AuNPs/MoS_2–GR/GCE, (e) thrombin/Apt1/AuNPs/MoS_2–GR/GCE, (f) QDs–Apt2/thrombin/Apt1/AuNPs/MoS_2–GR/GCE. (D) The ECL responses of the present ECL aptasensor to different concentrations of thrombin (pM). Inset in (B): the Randles equivalent circuit model for EIS. Inset in (D): linear calibration curve for thrombin. The electrolyte for CV and EIS detection: 1 M KCl + 5 mM $[Fe(CN)_6]^{3-/4-}$. The voltage rang in CV experiment is 0.6 to –0.2 V at a scan rate of 100 mV•s^{-1}. The frequency rang in EIS experiment is 1 Hz to 125 kHz. The electrolyte for ECL: 0.1 M pH 7.4 PBS solution (containing 0.02 M $K_2S_2O_8$ and 0.1 M KCl). The ECL signals were obtained under consecutive potential scanning from 0 to –1.7 V. The voltage of PMT: – 800V. Scan rate: 100 mV•s^{-1}.

Table 1 Comparison of the different sensors for thrombin detection

Sensors fabricated	Linear range (nM)	Detection limit (pM)	Ref.
aptamer/thrombin/aptamer–AuNPs	0.1–75	100	43
QDs/probe II/thrombin /probe I/Au electrode	27.2–545	2720	26
thrombin/TBA[a]/CM–PEG–CM[b]/APTES/GCE	0.001–160	0.0156	36
thrombin/FO[c]–Ru(phen)$_3^{2+}$/TBA[a]/GO–GCE	0.0009–0.226	0.40	37
AuNCs[d]–TBA[a] II–S1/thrombin/TBA[a] I/BSA/Au electrode	0.00001–5	0.0033	44
MB[e]–(THR–1)[f]/thrombin/BSA/ZnPc(OAr)$_4$[g]@SiO_2–(THR–2)[h]	0.25–5	80	45
Au NRs[i]–TBA[a]$_{29}$/thrombin/TBA[a]$_{15}$–$NaYF_4$:Yb,Er UCNPs[j]	2.5–90	1500	46
QDs–Apt2/thrombin/Apt1/AuNPs/MoS_2–GR/GCE	0.00002–0.005	0.0013	This work

a TBA, thrombin–binding aptamer.
b CM–PEG–CM, carboxymethyl–PEG–carboxymethyl.
c FO, functional oligonucleotide.
d AuNCs, gold nanoclusters.
e MB, magnetic beads
f THR–1, 5'–biotin GGT TGG TGT TGG
g ZnPc(OAr)$_4$, Tetra–α–(2,4–di–tert–butylphenoxy)–phthalocyaninato zinc
h THR–1, 5'–COOH AGT CCG TGG TAG GGC TTG GGG TGA CT
i Au NRs, gold nanorods

j UCNPs, upconversion nanoparticles

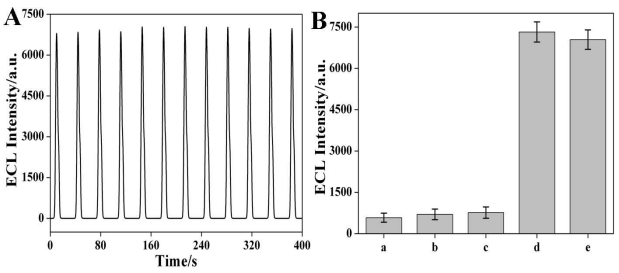

Fig. 4 The stability of the ECL aptasensor (A) and selectivity of the ECL aptasensor to the interfering proteins (B): 2.0×10^{-3} M HSA (column a), 1.0×10^{-6} M BSA (column b), 2.0×10^{-5} M human IgG (column c), 5 pM thrombin (column d), and the mixture of four proteins (column e). The ECL conditions are the same as in Fig. 3.

BSA (column b), and 2.0×10^{-5} M human IgG (column c) to replace 5 pM thrombin (column d) separately (Fig. 4B). Only weak ECL responses could be produced by replacing thrombin with HSA, BSA, and human IgG. The cross selectivity of the aptasensor in a mixture of above four different proteins was also examined (column e). The ECL response of thrombin in the mixture of four proteins had little difference with that in the pure thrombin solution, indicative of the good selectivity and accuracy of the prepared aptasensor.

Applications of the ECL aptasensor in human plasma analysis.

The applicability of the ECL aptasensor was evaluated by analyzing eight human plasma samples provided by Xinyang Central Hospital. The patients were divided into two groups, three non–traumatic injury patients (sample No. 1–3 in Table 2) and five traumatic injury patients (sample No. 4–8 in Table 2). The results from Table 2 showed that the contents of thrombin from traumatic injury patients are much higher that from non–traumatic injury patients. The recoveries of thrombin in plasma sample were also investigated. Three different concentrations of thrombin (0.04, 0.5, and 2.0 pM) were added into human plasma sample with recoveries of 90.0%, 92.4%, and 102.4%, respectively. The RSDs were less than 3.7%. These results demonstrate that the prepared ECL aptasensor is suitable for the analysis of thrombin in real biological samples.

Table 2 Analytical results of thrombin from eight human plasma samples

Sample	Thrombin content (pM)	Sample	Thrombin content (pM)
1	0.02	5	3.3
2	0.032	6	1.2
3	0.024	7	1.9
4	2.1	8	1.1

Conclusions

A novel and ultrasensitive ECL aptasensor was constructed based on layered MoS_2–GR composites and AuNPs for thrombin detection. Several advantages of this protocol with multiple signal amplification should be highlighted. Firstly, the 3D architecture of biointerface based on MoS_2–GR composites employed in the aptasensor could significantly improve the loading capacity and conductivity of GCE. Secondly, AuNPs assembled on the interface could conjugate the aptamer and greatly enhance the ECL signals. Thirdly, by coupling with the layered MoS_2–GR composites based biointerface and the QDs–aptamer nanoprobe, the fabricated sandwich–type ECL aptasensor exhibits attractive performances for detection of thrombin with very low detection limit, good selectivity, and acceptable stability. The protocol presents a new method for detection of proteins (e.g., tumor marker) in biological samples.

Acknowledgement

This work was supported by the National Natural Science Foundation of China (Grant 21375114, 21075106, U1304214) and the Foundation of Henan Educational Committee (14A150013).

Notes and references

[a]*College of Chemistry and Chemical Engineering, Xinyang Normal University, Xinyang 464000, China. E-mail: liuym9518@sina.com; Tel and Fax: +86-376-6392889.*
[b]*Xinyang Central Hospital, Xinyang 464000, China*

References

1. L. Kashefi–Kheyrabadi and M. A. Mehrgardi, *Bioelectrochemistry*, 2013, **94**, 47–52.
2. K. Sefah, J. A. Phillips, X. L. Xiong, L. Meng, D. V. Simaeys, H. Chen, J. Martin and W. H. Tan, *Analyst*, 2009, **134**, 1765–1775.
3. Y. Y. Qi and B. X. Li, *Chem.-Eur. J.*, 2011, **17**, 1642–1648.
4. K. M. Song, S. Lee and C. Ban, *Sensors*, 2012, **12**, 612–631.
5. Z. P. Yang, C. J. Zhang, J. X. Zhang and L. N. Huang, *Electrochim. Acta*, 2013, **111**, 25–30.
6. A. B. Iliuk, L. H. Hu and W. A. Tao, *Anal. Chem.*, 2011, **83**, 4440–4452.
7. Y. Chai, D. Y. Tian, J. Gu and H. Cui, *Analyst*, 2011, **136**, 3244–3251.
8. F. B. Lin, B. D. Yin, C. Z. Li, J. H. Deng, X. Y, Fan, Y. H. Yi, C. Liu, H. T. Li, Y. Y. Zhang and S. Z. Yao, *Anal. Methods*, 2013, **5**, 699–704.
9. N. Katiyar, L. S. Selvakumar, S. Patra and M. S. Thakur, *Anal. Methods*, 2013, **5**, 653–659.
10. H. K. Choi and J. H. Lee, *Anal. Methods*, 2013, **5**, 6964–6968.
11. D. Y. Liu, Y. Y. Xin, X. W. He and X. B. Yin, *Analyst*, 2011, **136**, 479–485.
12. H. Wang, C. X. Zhang, Y. Li and H. L. Qi, *Anal. Chim. Acta*, 2006, **575**, 205–211.
13. W. Zhan and A. J. Bard, *Anal. Chem.*, 2007, **79**, 459–463.
14. H. Y. Wang, W. Gong, Z. A. Tan, X. X. Yin and L. Wang, *Electrochim. Acta*, 2012, **76**, 416–423.
15. F. L. Yu, G. Li and C. M. Mao, *Electrochem. Commun.*, 2011, **13**, 1244–1247.
16. Y. M. Liu, Y. Yang, J. Li, L. F. Peng and L. Mei, *Curr. Anal. Chem.*, 2011, **7**, 325–332.
17. Y. M. Liu, J. Li, Y. Yang and J. J. Du, *Luminescence*, 2012, **28**, 673–678.
18. J. Zhou, N. Gan, F. T. Hu, T. H. Li, H. K. Zhou, X. Li and L. Zheng, *Sens. Actuators, B*, 2013, **186**, 300–307.
19. P. Bertoncello and R. J. Forster, *Biosens. Bioelectron.*, 2009, **24,** 3191–3200.
20. P. Bertoncello, *Front. Biosci.*, 2011, **16**, 1084–1108.
21. L. H. Zhang, L. Shang and S. J. Dong, *Electrochem. Commun.*, 2008, **10**, 1452–1454.
22. F. Divsar and H. X. Ju, *Chem. Commun.*, 2011, **47**, 9879–9881.

23. W. J. Miao, *Chem. Rev.*, 2008, **108**, 2506–2553.
24. M. Zhang, F. W. Wan, S. W. Wang, S. G. Ge, M. Yan and J. H. Yu, *J. Lumin.*, 2012, **132**, 938–943.
25. L. L. Li, K. P. Liu, G. H. Yang, C. M. Wang, J. R. Zhang and J. J. Zhu, *Adv. Funct. Mater.*, 2011, **21**, 869–878.
26. H. P. Huang and J. J. Zhu, *Biosens. Bioelectron.*, 2009, **25**, 927–930.
27. G. F. Jie, L. Wang, J. X. Yuan and S. S. Zhang, *Anal. Chem.*, 2011, **83**, 3873–3880.
28. H. S. S. R. Matte, A. Gomathi, A. K. Manna, D. J. Late, R. Datta, S. K. Pati and C. N. R. Rao, *Angew. Chem. Int. Ed.*, 2010, **49**, 4059–4062.
29. H. Hwang, H. Kim and J. Cho, *Nano Lett.*, 2011, **11**, 4826–4830.
30. J. M. Soon and K. P. Loh, *Electrochem. Solid–State Lett.*, 2007, **10**, A250–A254.
31. J. Chen, N. Kuriyama, H. T. Yuan, H. T. Takeshita and T. Sakai, J. *Amer. Chem. Soc.*, 2001, **123**, 11813–11814.
32. W. Choi, I. Lahiri, R. Seelaboyina and Y. S. Kang, *Crit. Rev. Solid State Mater. Sci.*, 2010, **35**, 52–71.
33. L. Ma, W. X. Chen, L. M. Xu, X. P. Zhou and B. Jin, *Ceram. Int.*, 2012, **38**, 229–234.
34. K. J. Huang, L. Wang, J. Li and Y. M. Liu, *Sens. Actuators, B*, 2013, **178**, 671–677.
35. S. Centi, S. Tombelli, M. Minunni and M. Mascini, *Anal. Chem.*, 2007, **79**, 1466–1473.
36. C. Sun, X. B. Wang, X. J. Yang, L. Xing, B. Zhao, X. D. Yang and C. Mao, *Electrochim. Acta*, 2013, **106**, 327–332.
37. X. Y. Wang, A. Gao, C. C. Lu, X. W. He and X. B. Yin, *Biosens. Bioelectron.*, 2013, **48**, 120–125.
38. W. S. Hummers and R. E. Offeman, *J. Amer. Chem. Soc.*, 1958, **80**, 1339–1339.
39. Y. L. Zhang, Y. Huang, J. H. Jiang, G. L. Shen and R. Q. Yu, *J. Amer. Chem. Soc.*, 2007, **129**, 15448–15449.
40. Y. M. Liu, L. Mei, L. J. Liu, L. F. Peng, Y. H. Chen and S. W. Ren, *Anal. Chem.*, 2011, **83**, 1137–1143.
41. X. Du, P. Guo, H. H. Song and X. H. Chen, *Electrochim. Acta*, 2010 **55**, 4812–4819.
42. N. Myung, Z. Ding and A. J. Bard, *Nano Lett.*, 2002, **2**, 1315–1319.
43. Y. F. Bai, F. Feng, L. Zhao, C. Y. Wang, H. Y. Wang, M. Z. Tian, J. Qin, Y. L. Duan and X. X. He, *Biosens. Bioelectron.*, 2013, **47**, 265–270.
44. J. Han, Y. Zhuo, Y. Q. Chai, G. F. Gui, M. Zhao, Q. Zhu and R. Yuan, *Biosens. Bioelectron.*, 2013, **50**, 161–166.
45. Z. Jiang, T. T. Yang, M. Y. Liu, Y. L. Hu and J. Wang, *Biosens. Bioelectron.*, 2014, **53**, 340–345.
46. H. Q. Chen, F. Yuan, S. Z. Wang, J. Xu, Y. Y. Zhang and L. Wang, *Biosens. Bioelectron.*, 2013, **48**, 19–25.